

Kirchhoff migration using eikonal-based computation of traveltimes source-derivatives^a

^aPublished in Geophysics, 78, no. 4, S211-S219, (2013)

Siwei Li and Sergey Fomel

ABSTRACT

The computational efficiency of Kirchhoff-type migration can be enhanced by employing accurate traveltimes interpolation algorithms. We address the problem of interpolating between a sparse source sampling by using the derivative of traveltimes with respect to the source location. We adopt a first-order partial differential equation that originates from differentiating the eikonal equation to compute the traveltimes source-derivatives efficiently and conveniently. Unlike methods that rely on finite-difference estimations, the accuracy of the eikonal-based derivative does not depend on input source sampling. For smooth velocity models, the first-order traveltimes source-derivatives enable a cubic Hermite traveltimes interpolation that takes into consideration the curvatures of local wave-fronts and can be straight-forwardly incorporated into Kirchhoff anti-aliasing schemes. We provide an implementation of the proposed method to first-arrival traveltimes by modifying the fast-marching eikonal solver. Several simple synthetic models and a semi-recursive Kirchhoff migration of the Marmousi model demonstrate the applicability of the proposed method.

INTRODUCTION

Over the years, there have been significant efforts and progress in traveltimes computations. The quality of traveltimes has a direct influence on Kirchhoff-type migrations since it determines the kinematic behaviors of the imaged wavefields. One can use either ray-tracing approaches or finite-difference solutions of the eikonal equation. The first option naturally handles multi-arrivals and can be extended to other wavefield approximations, such as Gaussian beams (Hill, 1990, 2001; Albertin et al., 2004; Gray, 2005), but is at the same time usually subject to the necessities of ray-coordinate and migration-grid mapping and irregular interpolation between rays in the presence of shadow zones in complex velocity media (Sava and Fomel, 1998). Two popular methods from the second option are the *fast-marching method* (FMM) (Sethian, 1996; Sethian and Popovici, 1999) and the *fast-sweeping method* (FSM) (Zhao, 2005). They both rely on an ordered update to recover the causality behind expanding wave-fronts in a general medium, and are thus limited to first-arrival computations. Several works attempt to overcome the single-arrival drawback of the finite-difference eikonal

solvers, for example multi-phase computation (Engquist and Runborg, 1996), phase-space escape equations (Fomel and Sethian, 2002), and slowness marching (Symes and Qian, 2003).

In practice, traveltime tables can be pre-computed on coarse grids and saved on disk, then serve as a dictionary when read by Kirchhoff migration algorithms. It is common to carry out a certain interpolation in this process in order to satisfy the needs of depth migration for fine-gridded traveltime tables at a large number of source locations (Mendes, 2000; Vanelle and Gajewski, 2002; Alkhalifah, 2011). Kirchhoff migrations with traveltime tables computed on the fly face the same issue. During the traveltime computation stage, accuracy requirements from eikonal solvers may lead to a fine model sampling. Combined with a large survey, traveltime computation for each shot can be costly. Because all traveltime computations handle one shot at a time, the overall cost increases linearly with the number of sources. Moreover, we need to store a large amount of traveltimes out of a dense source sampling. Therefore a sparse source sampling is preferred. In this paper, we try to address the problem of traveltime table interpolation between sparse source samples. The traveltime table estimated with simple nearest-neighbor or linear interpolation could not provide satisfying accuracy unless the velocity model has small variations. One possible improvement is to include derivatives in interpolation. During ray tracing, traveltime source-derivatives are directly connected to the slowness vector at the source and stay constant along individual rays, thus could be outputted as a by-product of traveltimes. For finite-difference eikonal solvers, such a convenience is not easily available. In these cases, we would like to avoid an extra differentiation on traveltime tables along the source dimension to compute such derivatives (Vanelle and Gajewski, 2002), because its accuracy in turn relies on a dense source sampling and induces additional computations. Alkhalifah and Fomel (2010) derived an equation for the traveltime perturbation with respect to the source location changes. The governing equation is a first-order partial differential equation (PDE) that describes traveltime source-derivatives in a relative coordinate moving along with the source. In this paper, we show that the traveltime source-derivative desired by interpolation is related to this relative-coordinate quantity by a simple subtraction with the slowness vector. Unlike a finite-difference approach, traveltime source-derivatives computed by the PDE method are source-sampling independent. The extra costs are rather inexpensive. In this paper, we apply this method to Kirchhoff migration with first-arrival traveltimes computed by the FMM eikonal solver.

The paper is organized as follows. In the first section, we review the theory and implementation of the eikonal-based traveltime source-derivatives. Next, we use both simple and complex synthetic models to demonstrate the accuracy of a cubic Hermite traveltime table interpolation using the source-derivatives, and show effects of incorporating such an interpolation into Kirchhoff migration. We focus mainly on the kinematics in these experiments by neglecting possible true-amplitude weights in Kirchhoff migration. Finally, we discuss limitations and possible extensions of the proposed method.

THEORY AND IMPLEMENTATION

We consider the isotropic eikonal equation:

$$\nabla T(\mathbf{x}) \cdot \nabla T(\mathbf{x}) = \frac{1}{v^2(\mathbf{x})} \equiv W(\mathbf{x}), \quad (1)$$

where \mathbf{x} is a point in space, $T(\mathbf{x})$ is the traveltime and $v(\mathbf{x})$ is the velocity. For 2D models, \mathbf{x} is a vector containing the depth and the inline position. For 3D models, \mathbf{x} also includes the crossline position. For conciseness, we define $W(\mathbf{x})$ as slowness-squared. Equation 1 can be derived by inserting the ray-theory series into the wave-equation and setting the coefficient of the leading-order term to zero (Chapman, 2004). We are interested in particular in point-source solutions of the eikonal equation, i.e. with the initial condition $T(\mathbf{x}_s) = 0$ where \mathbf{x}_s denotes the source location.

Traveltime Source-derivative

The point-source traveltime $T(\mathbf{x})$ clearly depends on the source location \mathbf{x}_s . To explicitly show such a dependency in the eikonal equation, we define a relative coordinate \mathbf{q} as

$$\mathbf{q} = \mathbf{x} - \mathbf{x}_s, \quad (2)$$

and use $\hat{T}(\mathbf{q}; \mathbf{x}_s)$ to denote traveltime in the relative coordinates. After inserting this definition into equation 1, we obtain

$$\nabla_{\mathbf{q}} \hat{T} \cdot \nabla_{\mathbf{q}} \hat{T} = W(\mathbf{q} + \mathbf{x}_s). \quad (3)$$

Here the differentiation $\nabla_{\mathbf{q}}$ stands for gradient operator in the relative coordinate \mathbf{q} and is taken with a fixed source location \mathbf{x}_s . In 3D, if $\mathbf{q} = (q_1, q_2, q_3)$ and denoting \mathbf{e}_i with $i = \{1, 2, 3\}$ to be the unit vector in depth, inline and crossline directions, respectively, then

$$\nabla_{\mathbf{q}} \equiv \frac{\partial}{\partial q_1} \mathbf{e}_1 + \frac{\partial}{\partial q_2} \mathbf{e}_2 + \frac{\partial}{\partial q_3} \mathbf{e}_3. \quad (4)$$

Since we are interested in the traveltime derivative with respect to the source, i.e. $\partial T / \partial \mathbf{x}_s$, we take directional derivative $\partial / \partial \mathbf{x}_s$ to $\hat{T}(\mathbf{q}; \mathbf{x}_s)$ and apply the chain-rule according to equation 2:

$$\frac{\partial T}{\partial \mathbf{x}_s} \equiv \frac{\partial \hat{T}}{\partial \mathbf{x}_s} = \frac{\partial \hat{T}}{\partial \mathbf{x}} \frac{\partial \mathbf{x}}{\partial \mathbf{x}_s} + \frac{\partial \hat{T}}{\partial \mathbf{q}} \frac{\partial \mathbf{q}}{\partial \mathbf{x}_s} = \frac{\partial \hat{T}}{\partial \mathbf{x}} - \frac{\partial \hat{T}}{\partial \mathbf{q}}. \quad (5)$$

Equation 5 results in a vector that contains the traveltime source-derivatives in depth, inline and crossline directions. In accordance with $\partial / \partial \mathbf{x}_s$, $\partial / \partial \mathbf{x}$ and $\partial / \partial \mathbf{q}$ are also directional derivatives. All numerical examples in this paper are based on a typical 2D acquisition, where we assume a constant source depth and thus only the inline traveltime source-derivative is of interest. The quantity $\partial \hat{T} / \partial \mathbf{q}$ coincides with the

slowness vector of the ray that originates from \mathbf{x}_s . For a finite-difference eikonal solver such as FMM and FSM, it is usually estimated by an upwind scheme during traveltime computations at each grid point and thus can be easily extracted. Applying $\partial/\partial\mathbf{x}$ to both sides of equation 3, we find

$$\nabla_{\mathbf{q}}\hat{T} \cdot \nabla_{\mathbf{q}}\frac{\partial\hat{T}}{\partial\mathbf{x}} = \frac{1}{2}\frac{\partial W}{\partial\mathbf{x}}. \quad (6)$$

Equation 6 has the form of the linearized eikonal equation (Aldridge, 1994) and was previously derived, in a slightly different notation, by Alkhalifah and Fomel (2010). It implies that $\partial\hat{T}/\partial\mathbf{x}$, as needed by equation 5, can be determined along the characteristics of \hat{T} . Since the right-hand side contains a slowness-squared derivative, the velocity model must be differentiable, as is usually required by traveltime computations. The derivation also indicates that the accuracy of an eikonal-based traveltime source-derivative is source-sampling independent but model-sampling dependent, as from equations 5 and 6 $\partial/\partial\mathbf{x}_s$ relies on \hat{T} , $\partial/\partial\mathbf{q}$ and $\partial/\partial\mathbf{x}$. The accuracy from a direct finite-difference estimation on $\partial/\partial\mathbf{x}_s$, in comparison, is both source- and model-sampling dependent.

Continuing applying differentiation and the chain-rule to equation 5 will result in higher-order traveltime source-derivatives. For example, the second-order derivative reads:

$$\begin{aligned} \frac{\partial^2 T}{\partial\mathbf{x}_s^2} &\equiv \frac{\partial^2\hat{T}}{\partial\mathbf{x}_s^2} = \frac{\partial}{\partial\mathbf{x}}\frac{\partial\hat{T}}{\partial\mathbf{x}} \cdot \frac{\partial\mathbf{x}}{\partial\mathbf{x}_s} + \frac{\partial}{\partial\mathbf{q}}\frac{\partial\hat{T}}{\partial\mathbf{x}} \cdot \frac{\partial\mathbf{q}}{\partial\mathbf{x}_s} - \frac{\partial}{\partial\mathbf{x}}\frac{\partial\hat{T}}{\partial\mathbf{q}} \cdot \frac{\partial\mathbf{x}}{\partial\mathbf{x}_s} - \frac{\partial}{\partial\mathbf{q}}\frac{\partial\hat{T}}{\partial\mathbf{q}} \cdot \frac{\partial\mathbf{q}}{\partial\mathbf{x}_s} \\ &= \frac{\partial^2\hat{T}}{\partial\mathbf{x}^2} - 2\frac{\partial^2\hat{T}}{\partial\mathbf{x}\partial\mathbf{q}} + \frac{\partial^2\hat{T}}{\partial\mathbf{q}^2}. \end{aligned} \quad (7)$$

Further, differentiating equation 6 once more by \mathbf{x} provides

$$\nabla_{\mathbf{q}}\frac{\partial\hat{T}}{\partial\mathbf{x}} \cdot \nabla_{\mathbf{q}}\frac{\partial\hat{T}}{\partial\mathbf{x}} + \nabla_{\mathbf{q}}\hat{T} \cdot \nabla_{\mathbf{q}}\frac{\partial^2\hat{T}}{\partial\mathbf{x}^2} = \frac{1}{2}\frac{\partial^2 W}{\partial\mathbf{x}^2}. \quad (8)$$

It is easy to verify that any order of the traveltime source-derivative will require the corresponding order of the slowness-squared derivative. An approximation based on Taylor expansions of the traveltime around a fixed source location can make use of these derivatives. For example, Ursin (1982) and Bortfeld (1989) introduced parabolic and hyperbolic traveltime approximations with the first- and second-order derivatives. Notice that the need for slowness-squared derivatives may cause instability unless the velocity model is sufficiently smooth. Alkhalifah and Fomel (2010) also proved the following relationship between $\partial W/\partial\mathbf{x}$ and $\partial\hat{T}/\partial\mathbf{q}$:

$$\nabla_{\mathbf{q}}\hat{T} \cdot \nabla_{\mathbf{q}}\frac{\partial\hat{T}}{\partial(\mathbf{q} + \mathbf{x}_s)} = \frac{1}{2}\frac{\partial W}{\partial\mathbf{x}}, \quad (9)$$

which implies that the traveltime source-derivative can be computed from the given traveltime tables only. However, the velocity smoothness is still implicitly assumed

as the second-order spatial derivatives of traveltimes appear in the equation. For this reason, we restrict our current implementation to the first-order derivative only.

In a ray-tracing eikonal solver, $\partial T/\partial \mathbf{x}_s$ is the slowness vector of a particular ray at \mathbf{x}_s and holds constant along the trajectory. As it may also require irregular coordinate mappings, one may use the same strategy as for the traveltime tables. In this way, there is no necessity for any additional effort. On the other hand, equations 5 and 6 and their second-order extensions provide important attributes for use in Gaussian beams, which are commonly calculated by the dynamic ray tracing (Červený, 2001). They might be alternatively estimated by the eikonal-based source-derivative formulas but with the traveltime tables from a finite-difference eikonal solver. However, this application is beyond the scope of this paper. In the following sections, we consider only the source-derivative estimation from traveltimes computed by a finite-difference eikonal solver.

Numerical Implementation

Equation 6 is a linear first-order PDE suitable for upwind numerical methods (Franklin and Harris, 2001). Since it does not change the non-linear nature of the eikonal equation, the resulting traveltime source-derivative can be related to any branch of multi-arrivals, if one supplies the corresponding traveltime in \hat{T} . The source-derivatives can be computed either along with traveltimes or separately. In Appendix A, we describe a first-arrival implementation based on a modification of FMM (Sethian, 1996).

The first-order traveltime source-derivative enables a cubic Hermite interpolation (Press et al., 2007). Geometrically, such an interpolation is valid only when the selected wave-front in the interpolation interval is smooth and continuous. For a 2D model and a source interpolation along the inline direction only, the Hermite interpolation reads:

$$\begin{aligned} T(z, x; z_s, x_s + \alpha \Delta x_s) &= (2\alpha^3 - 3\alpha^2 + 1) T(z, x; z_s, x_s) \\ &+ (\alpha^3 - 2\alpha^2 + \alpha) \frac{\partial T}{\partial x_s}(z, x; z_s, x_s) \\ &+ (-2\alpha^3 + 3\alpha^2) T(z, x; z_s, x_s + \Delta x_s) \\ &+ (\alpha^3 - \alpha^2) \frac{\partial T}{\partial x_s}(z, x; z_s, x_s + \Delta x_s), \end{aligned} \quad (10)$$

where $\alpha \in [0, 1]$ controls the source position to be interpolated between known values at (z_s, x_s) and $(z_s, x_s + \Delta x_s)$. For comparison, the linear interpolation can be represented by:

$$T(z, x; z_s, x_s + \alpha \Delta x_s) = (1 - \alpha) T(z, x; z_s, x_s) + \alpha T(z, x; z_s, x_s + \Delta x_s). \quad (11)$$

The linear interpolation fixes the subsurface image point (z, x) . A possible improvement is to instead fix the vector that links the source with the image, such that on the right-hand side the traveltimes are taken at shifted image locations:

$$\begin{aligned} T(z, x; z_s, x_s + \alpha \Delta x_s) &= (1 - \alpha) T(z, x - \alpha \Delta x_s; z_s, x_s) \\ &+ \alpha T(z, x + (1 - \alpha) \Delta x_s; z_s, x_s + \Delta x_s). \end{aligned} \quad (12)$$

We will refer to scheme 12 as shift interpolation. According to our definition of the relative coordinate \mathbf{q} in equation 2, shift interpolation amounts to a linear interpolation in $\hat{T}(\mathbf{q}; \mathbf{x}_s)$. It is easy to verify that, for a constant-velocity medium, both Hermite and shift interpolations are accurate, while the linear interpolation is not. However, the accuracy of shift interpolation deteriorates with increasing velocity variations, as it assumes that the wave-front remains invariant in the relative coordinate. Equations 10-12 can be generalized to 3D by cascading the inline and crossline interpolations (for example equation 11 in 3D case becomes bilinear interpolation). The interpolated source does not need to lie collinear with source samples.

The derivatives themselves can also be directly used for Kirchhoff anti-aliasing (Lumley et al., 1994; Abma et al., 1999; Fomel, 2002). Equations 10, 11 and 12 give rise to their corresponding source-derivative interpolations after applying the following chain-rule to both sides:

$$\frac{\partial}{\partial(x_s + \alpha\Delta x_s)} = \frac{\partial}{\partial\alpha} \frac{\partial\alpha}{\partial(x_s + \alpha\Delta x_s)} = \frac{1}{\Delta x_s} \frac{\partial}{\partial\alpha}. \quad (13)$$

The anti-aliasing application is summarized in Appendix B.

NUMERICAL EXAMPLES

Constant-velocity-gradient Model

In a 2D medium of linearly changing velocities, $v(z, x) = v_0 + ax + bz$ where x is the lateral position and z is the depth, the traveltimes and source-derivatives have analytical solutions (Slotnick, 1959). Figure 1 shows the model used in our numerical test and the analytical source-derivative for a source located at $(0, 0)$ km. The domain is of size $4\text{km} \times 4\text{km}$ with grid spacing 0.01 km in both directions. We solve for the traveltimes tables at five sources of uniform spacing 1 km along the top domain boundary by FMM and their associated source-derivatives using the method described in Appendix A. Figure 2 compares the errors in computed source-derivative between the proposed approach and a centered second-order finite-difference estimation for the same source shown in Figure 1. The proposed method is sufficiently accurate except for the small region around the source. This is due to the source singularity of the eikonal equation and can be improved by adaptive or high-order upwind finite-difference methods (Qian and Symes, 2002) or by factoring the singularity (Fomel et al., 2009). Since we are aiming at using the interpolated traveltimes tables for migration purposes and the reflection energy around the sources is usually low, these errors in current implementation can be neglected. In Figure 3, we interpolate the traveltimes table for a source at location $(0, 0.25)$ km from the nearby source samples at $(0, 0)$ km and $(0, 1)$ km by the cubic Hermite, linear and shift interpolations. We use the eikonal-based source-derivative in the cubic Hermite interpolation. The shift interpolation is not applicable for some \mathbf{q} and \mathbf{x}_s if $\mathbf{x} = \mathbf{q} + \mathbf{x}_s$ is beyond the computational domain. In these regions, we use a linear interpolation to fill the traveltimes

table. As expected, the cubic Hermite interpolation achieves the best result, while its misfits near the source are related to the errors in source-derivatives. The shift interpolation performs generally better than the linear interpolation, especially in the regions close to the source where the wave-fronts are simple.

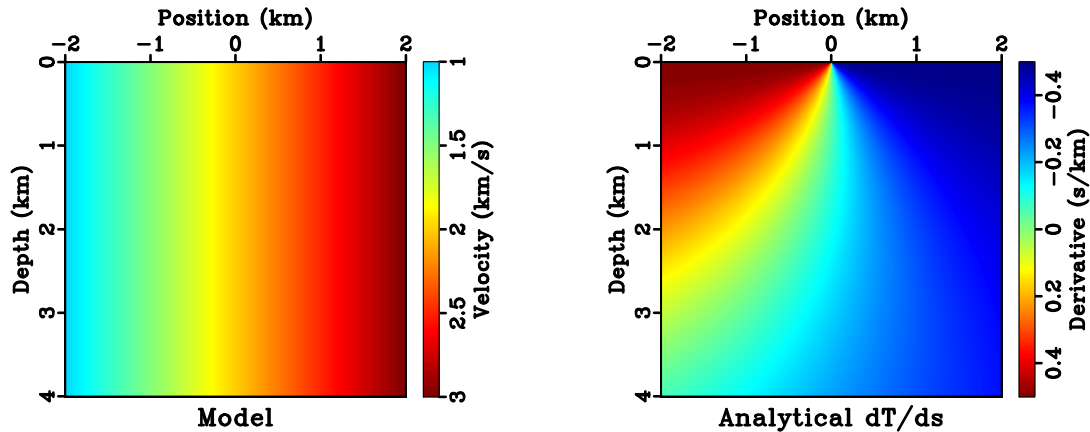


Figure 1: (Left) a constant-velocity-gradient model $v(z, x) = 2 + 0.5x$ km/s and (right) its analytical traveltime source-derivative for a source at origin $\mathbf{x}_s = (0, 0)$ km.

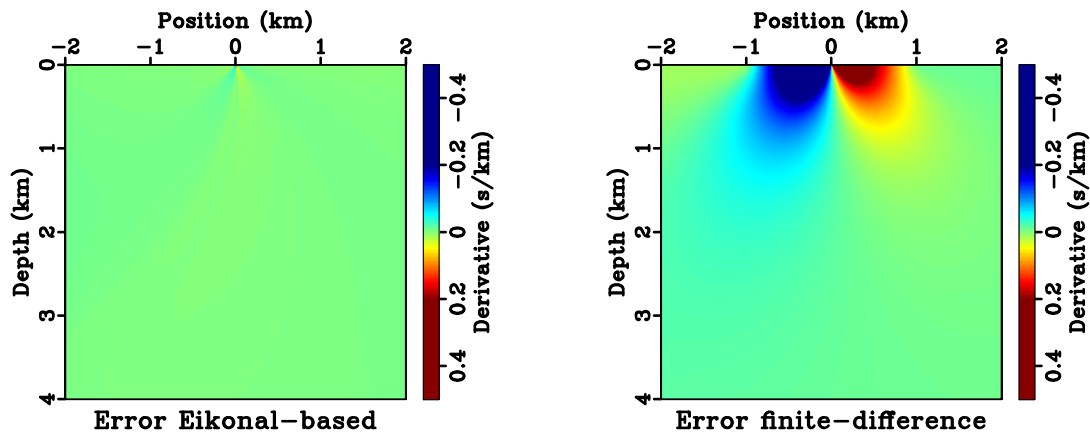


Figure 2: Comparison of error in computed source-derivative by (left) the proposed method and (right) a centered second-order finite-difference estimation based on traveltime tables. The maximum absolute errors are 0.15 s/km and 0.56 s/km, respectively.

The difference between a cubic Hermite interpolation and a linear or shift one is in the usage of source-derivatives. In this regard, one may think of supplying the finite-difference estimated derivatives to the interpolation. Indeed, a refined source sampling and higher-order differentiation may lead to more accurate derivatives. However the additional computation is considerable. For the same model in Figure 1, we carry out both a source sampling refinement experiment and a model grid spacing refinement

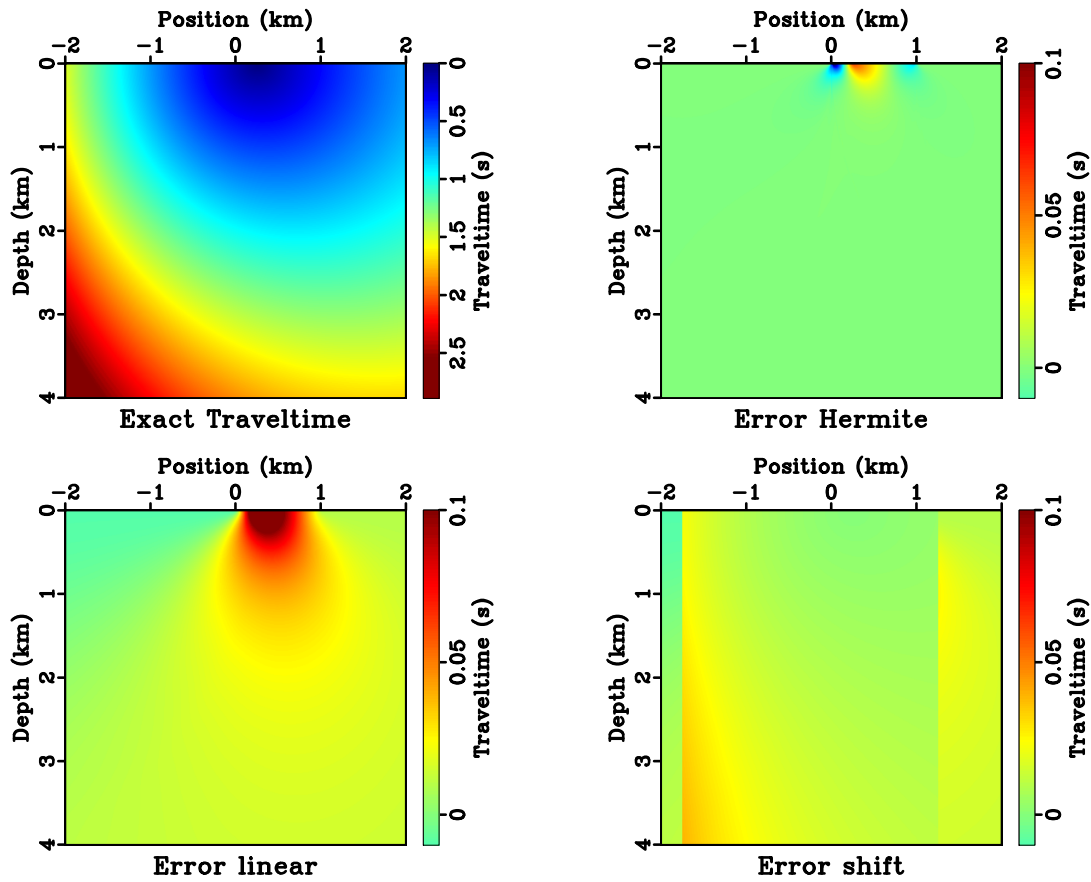


Figure 3: Traveltime interpolation error of three different schemes: (top left) the analytical traveltime of a source at location $(0, 0.25)$ km; (top right) error of the cubic Hermite interpolation; (bottom left) error of the linear interpolation; (bottom right) error of the shift interpolation. Using derivatives in interpolation enables a significantly higher accuracy. The l_2 norm of the error are 1.5 s, 9.2 s and 6.0 s respectively.

experiment. The results are shown in Figures 4 and 5. Both figures are plotted for the traveltime at subsurface location $(1.5, -0.5)$ km for the source at location $(0, 0)$ km. Although the curves vary for different locations, the source sampling refinement experiment suggests the general need for approximately three times finer source-sampling than that of Figure 2 to achieve the same level of accuracy.

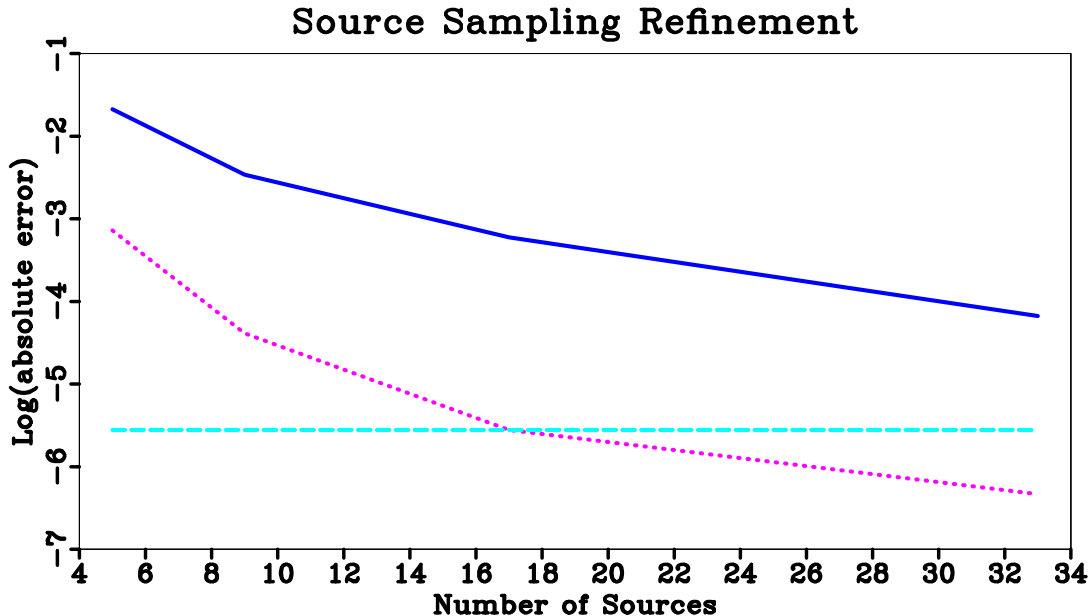


Figure 4: Source-sampling refinement experiment. The plot shows, at a fixed model grid sampling of 0.01 km and increasing source sampling, the error in source-derivative estimated by a first-order finite-difference (solid) and a centered second-order finite-difference scheme (dotted) decrease. The horizontal axis is the number of sources and the source sampling is uniform. The vertical axis is the natural logarithm of the absolute error. The flat line (dash) is from the proposed eikonal-based method and is source-sampling independent.

Kirchhoff migration can use traveltime source-derivatives in two ways: for traveltime interpolation when the source and receiver of a trace does not lie on the source grid of pre-computed traveltime tables, and for anti-aliasing. Figure 6 shows a synthetic model of constant-velocity-gradient with five dome-shaped reflectors. The model has a 0.01 km grid spacing in both directions. We solve for traveltimes and source-derivatives by the modified FMM introduced in Appendix A at 21 sparse shots of uniform spacing 0.5 km, and migrate synthetic zero-offset data. The interpolation of source-derivative for the anti-aliasing purpose follows the method described in Appendix B. 48 interpolations are carried out within each sparse source sampling interval. Figures 7 and 8 compare the images obtained by three different interpolations and the effect of anti-aliasing. All images are plotted at the same scale. We do not limit migration aperture for all cases and adopt the anti-aliasing criteria suggested by Abma et al. (1999) to filter the input trace before mapping a sample to the image, where the source-derivative and receiver-derivative (in the zero-offset case they coin-

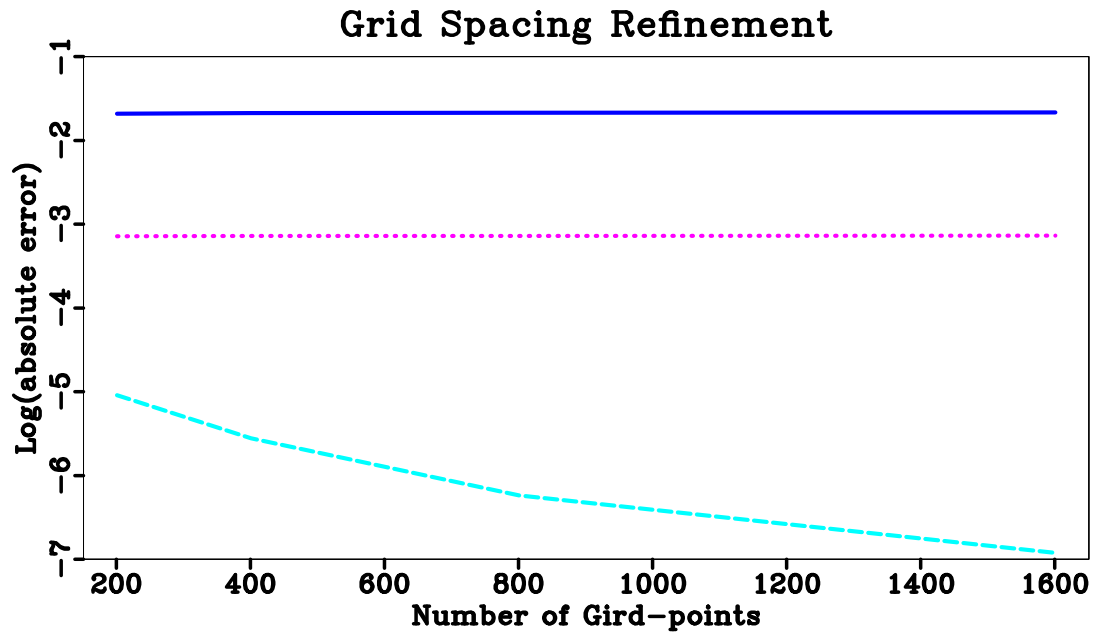


Figure 5: Grid-spacing refinement experiment. The plot shows, at a fixed source sampling of 1 km and increasing model grid sampling, the error in source-derivative estimated by the proposed eikonal-based method decreases. Meanwhile, the errors of both first- and second-order finite-difference estimations do not improve noticeably. The horizontal axis is the number of grid points in both directions and the grid sampling is uniform. See Figure 4 for descriptions of the vertical axis and the lines.

cide) determine the filter coefficients. As expected, the cubic Hermite interpolation with anti-aliasing leads to the most desirable image. The image could be further improved by considering not only the kinematics predicted by the traveltimes but also the amplitude factors (Dellinger et al., 2000; Vanelle et al., 2006).

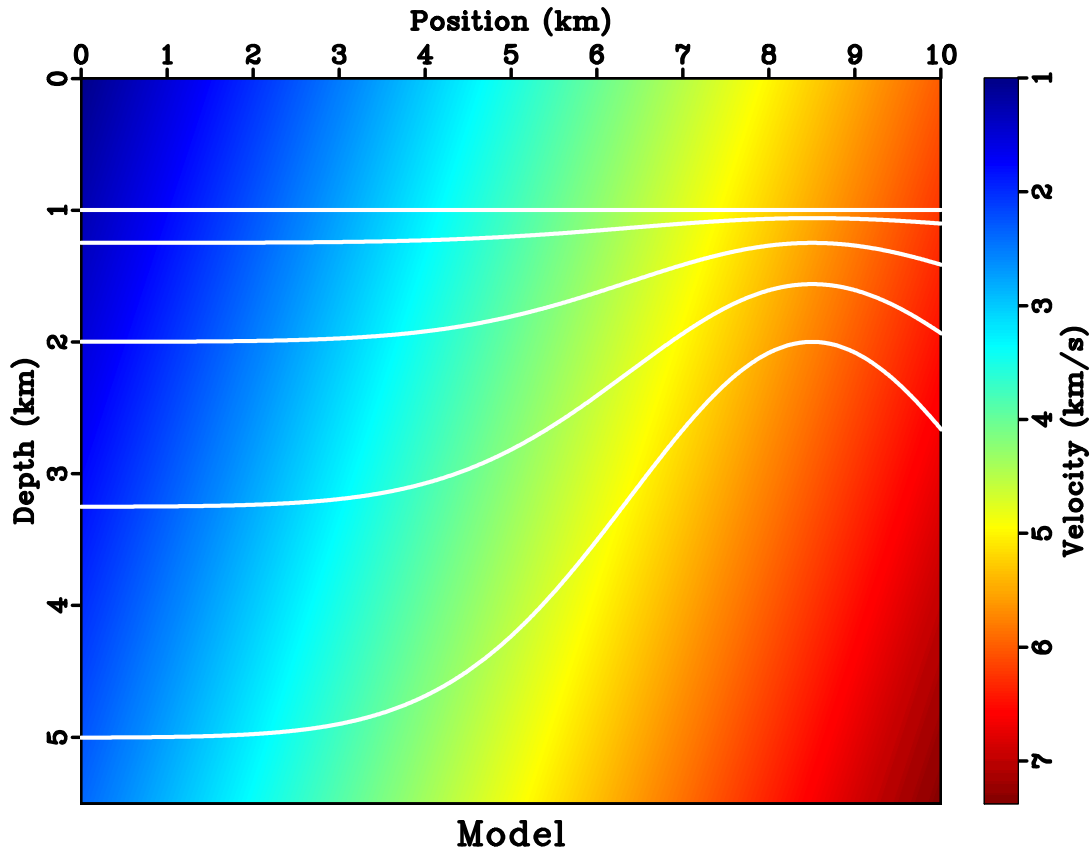


Figure 6: Constant-velocity-gradient background model $v(z, x) = 1.5 + 0.25z + 0.25x$ km/s with dome shaped reflectors.

Marmousi Model

The Marmousi model (Versteeg, 1994) has large velocity variations and is challenging for Kirchhoff migration with first-arrivals (Geoltrain and Brac, 1993). We apply a single-fold 2D triangular smoothing of radius 20 m to the original model (see Figure 9) to remove only sharp velocity discontinuities but retain the complex velocity structures. Because wave-fronts change shapes rapidly, the traveltime interpolation may be subject to inaccurate source-derivatives and provide less satisfying accuracy compared to that in a simple model. Although the derivative computation in the proposed eikonal-based method is source-sampling independent, in practice we should limit the interpolation interval to be sufficiently small, so that the traveltime curve could be well represented by a cubic spline. For the smoothed Marmousi model, we

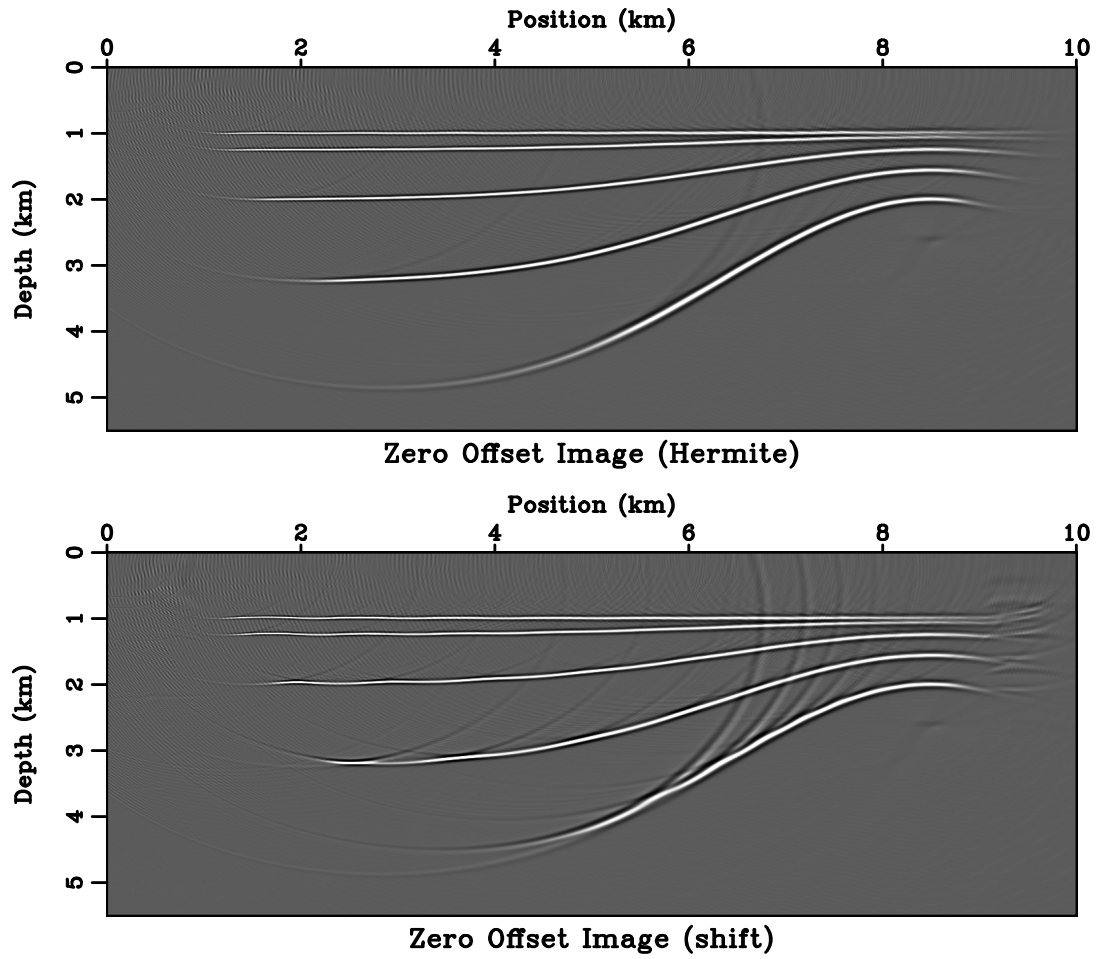


Figure 7: Zero-offset Kirchhoff migration image with (top) the cubic Hermite interpolation and (bottom) the shift interpolation.

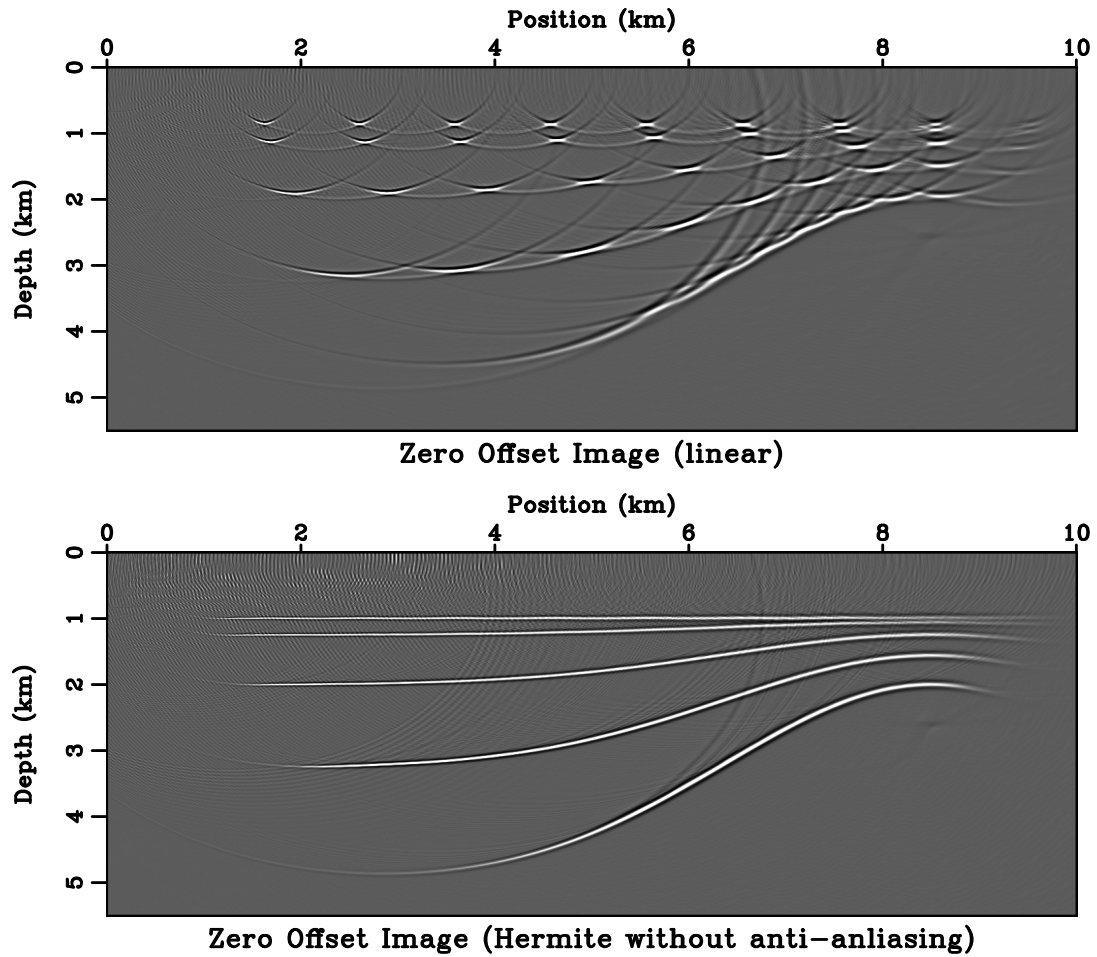


Figure 8: Zero-offset Kirchhoff migration image with (top) the linear interpolation and (bottom) the cubic Hermite interpolation without anti-aliasing.

use a sparse source sampling of 0.2 km based on observations of the horizontal width of major velocity structures. Figures 9 and 10 compare the traveltime interpolation errors of three methods as in Figure 3 for a source located at (0, 3.1) km from nearby source samples at (0, 3) km and (0, 3.2) km. Figure 11 plots a reference traveltime curve for the fixed subsurface location (2, 3.3) km computed by a dense eikonal solving of 4 m source spacing against curves produced by the interpolations. While these comparisons vary between different source intervals and subsurface locations, the cubic Hermite interpolation out-performs the linear and the shift interpolations except for the source singularity region. However in Figure 9 the errors are relatively large in the upper-left region. These errors occur due to the collapse of overlapping branches of the traveltime field (Xu et al., 2001) that causes wave-front discontinuities and undermines the assumptions of the proposed method.

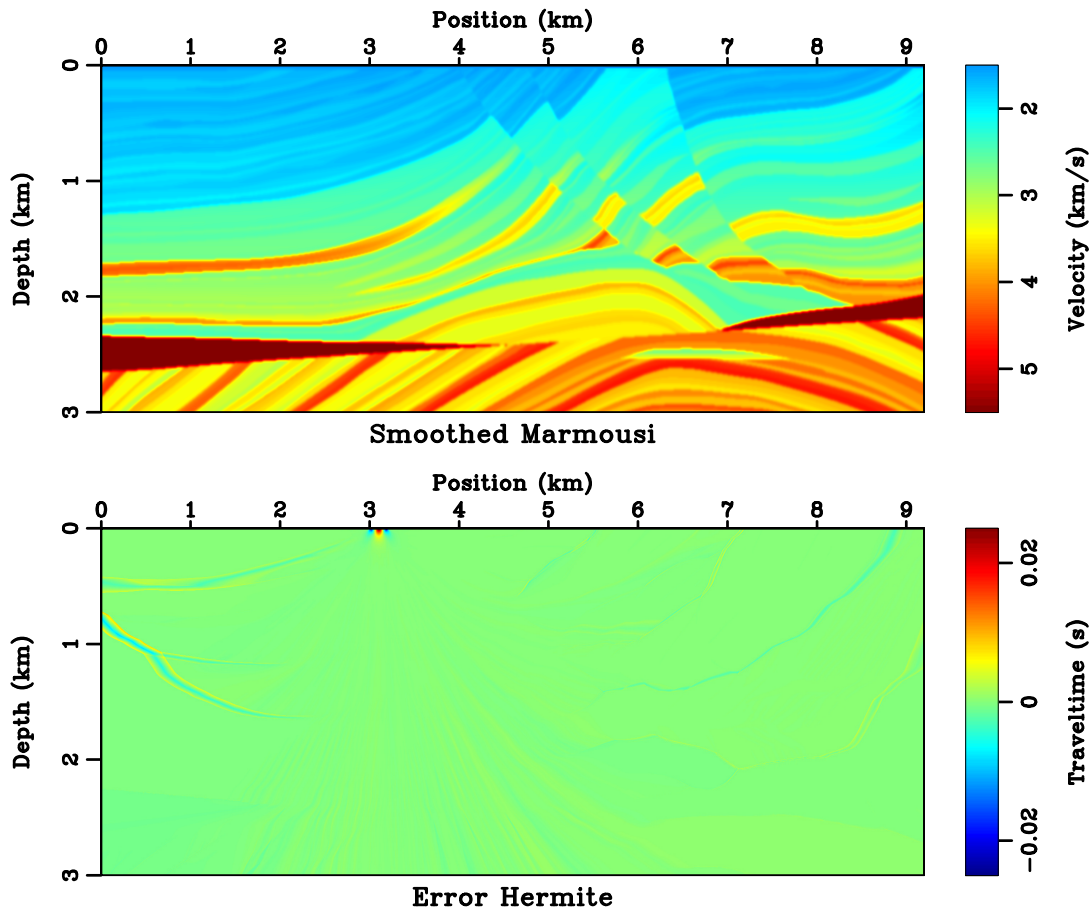


Figure 9: (Top) the smoothed Marmousi model. The model has a 4 m fine grid. (Bottom) the traveltime error by the cubic Hermite interpolation.

One strategy for imaging multi-arrival wavefields with first-arrival traveltimes is the semi-recursive Kirchhoff migration (Bevc, 1997). It breaks the image into several depth intervals, applies Kirchhoff redatuming to the next interval, performs Kirchhoff migration from there, and so on. The small redatuming depth effectively limits

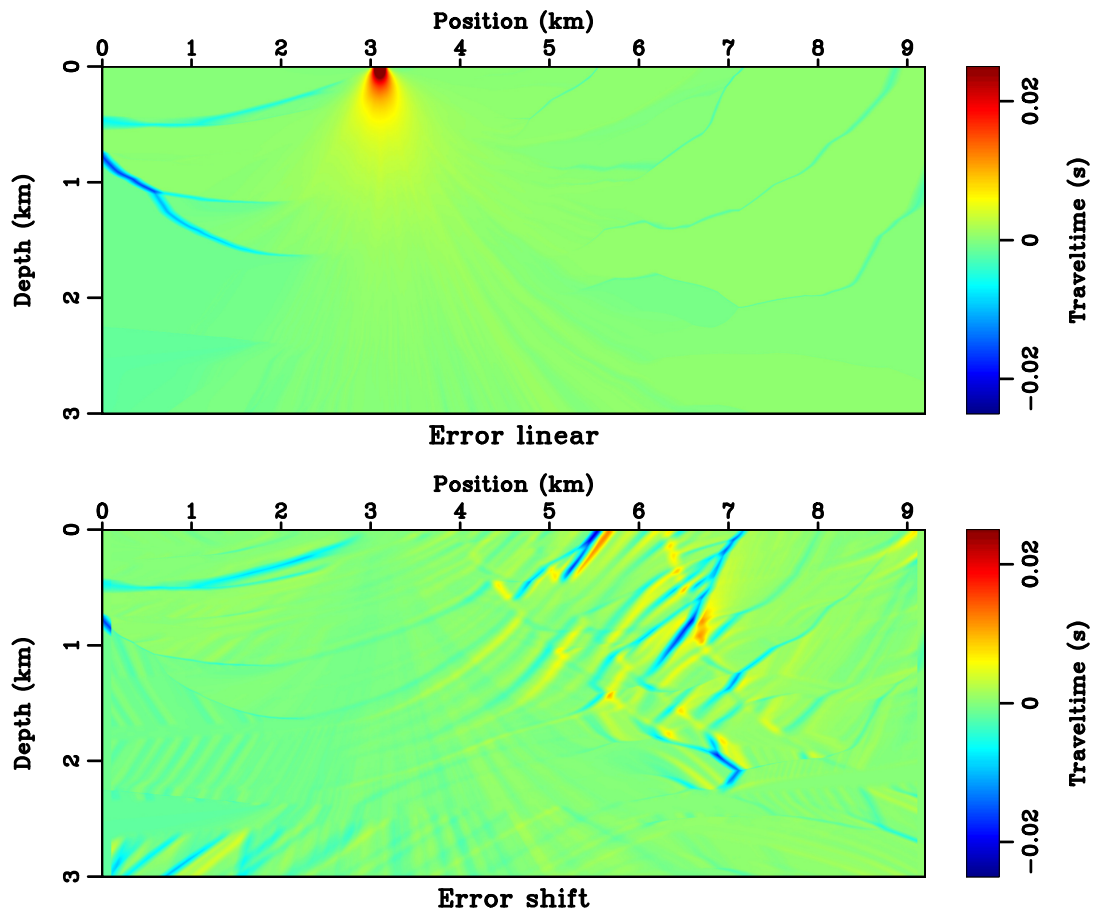


Figure 10: The traveltime error by (top) the linear interpolation and (bottom) the shift interpolation.

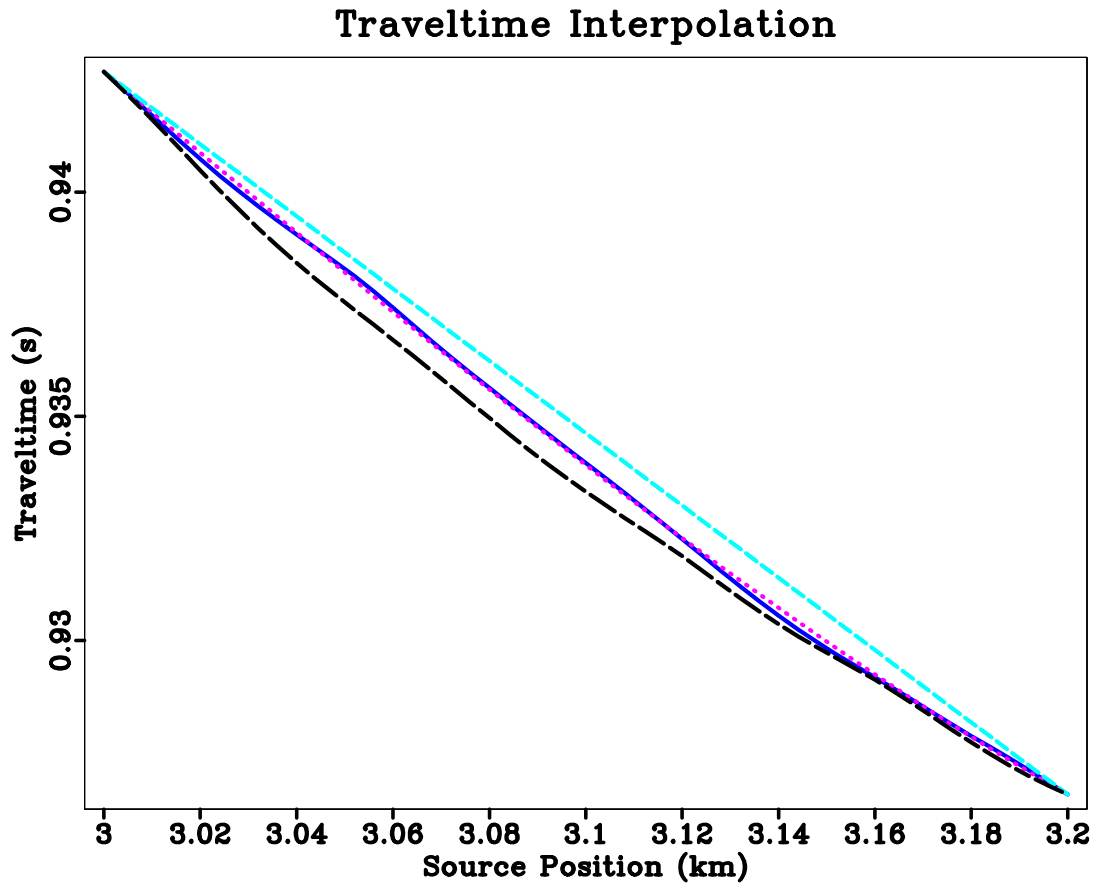


Figure 11: Traveltime interpolation for a fixed subsurface location. Compare between the result from a dense source sampling (solid blue), cubic Hermite interpolation (dotted magenta), linear interpolation (dashed cyan) and shift interpolation (dashed black). The l_2 norm of the error (against the dense source sampling results) of 49 evenly interpolated sources between interval (0, 3) km and (0, 3.2) km for all locations but the top 100 m source singularity region are 3.9 s, 9.2 s and 11.6 s respectively.

the maximum traveltimes and the evolving of complex waveforms before the most energetic arrivals separate from first-arrivals. Since Kirchhoff redatuming also relies on traveltimes between datum levels, our method can be fully incorporated into the whole process. Again, for simplicity, we do not consider amplitude factors during migration. We use the Marmousi dataset with a source/receiver sampling of 25 m. Due to the source and receiver reciprocity, the receiver side interpolations are equivalent to those on the source side. Figure 12 is the result of a Kirchhoff migration with eikonal solvings at each source/receiver location, i.e. no interpolation performed. Only the upper portion is well imaged. Figure 13 shows the image after employing the cubic Hermite interpolation with a 0.2 km sparse source/receiver sampling, which means 7 source interpolations within each interval. Even though a 7 times speed-up is not attainable in practice due to the extra computations in source-derivative and interpolation, we are still able to gain an approximately 5-fold cost reduction in traveltimes computations, while keeping the image quality comparable between Figures 12 and 13. Next, following Bevc (1997), we downward continue the data to a depth of 1.5 km in three datuming steps. The downward continued data are then Kirchhoff migrated and combined with the upper portion of Figure 13. We keep the same 0.2 km sparse source/receiver sampling whenever eikonal solvings are required in this process. Figure 14 shows the image obtained by the semi-recursive Kirchhoff migration. The target zone at approximately (2.5, 6.5) km appears better imaged.

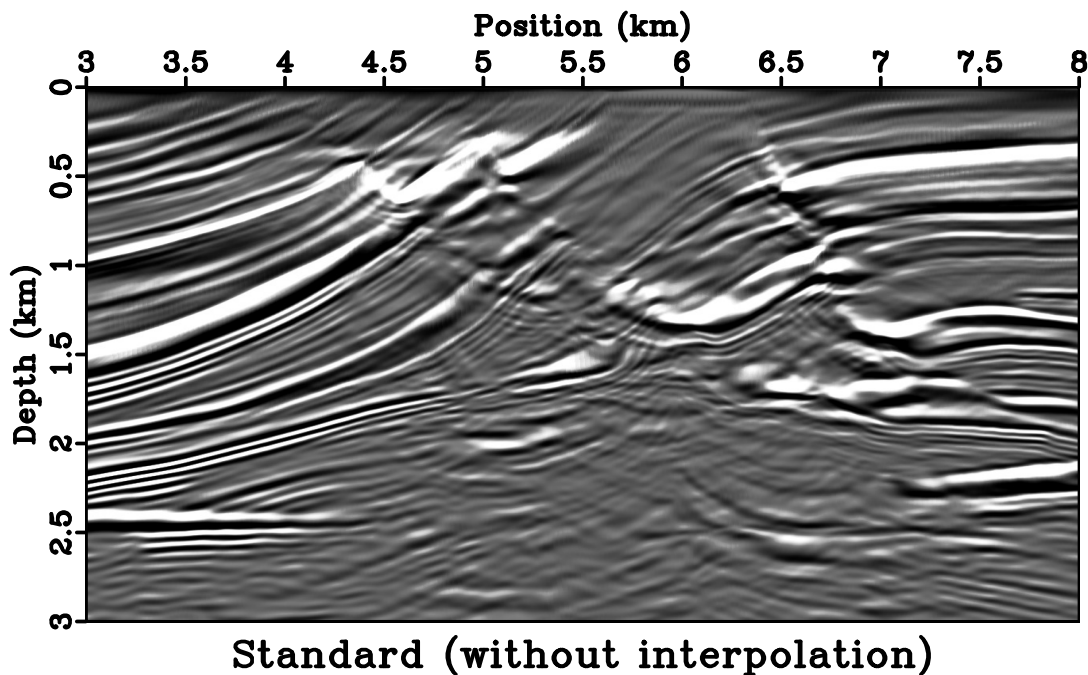


Figure 12: Image of Kirchhoff migration with first-arrivals (no interpolation).

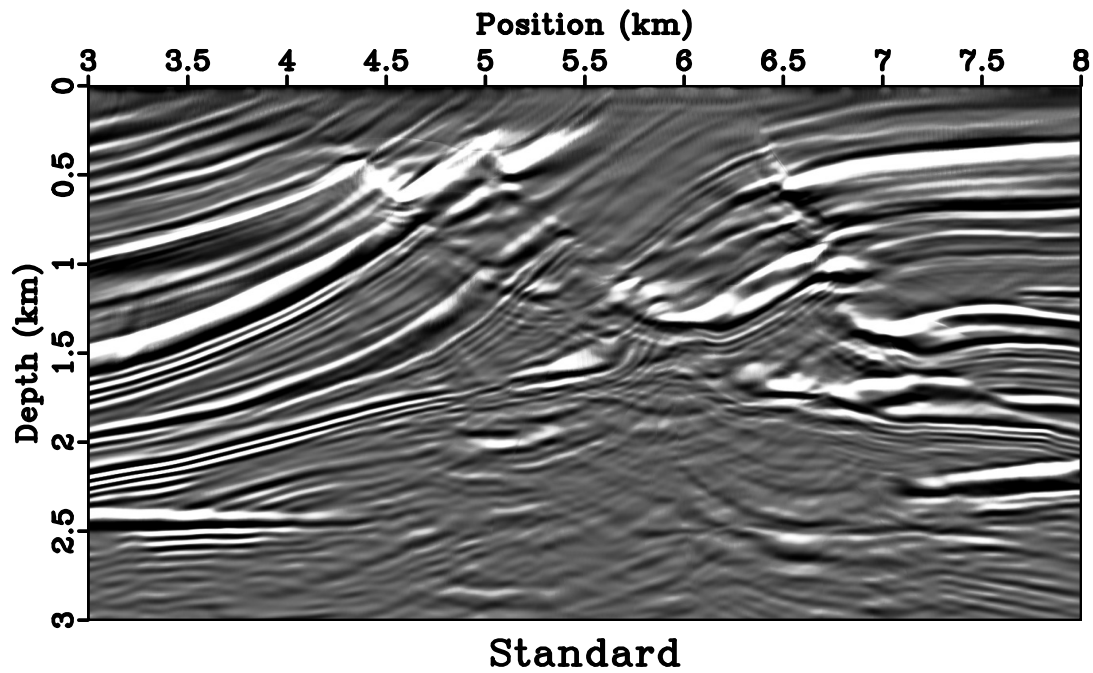


Figure 13: Image of Kirchhoff migration with first-arrivals and a sparse source/receiver sampling.

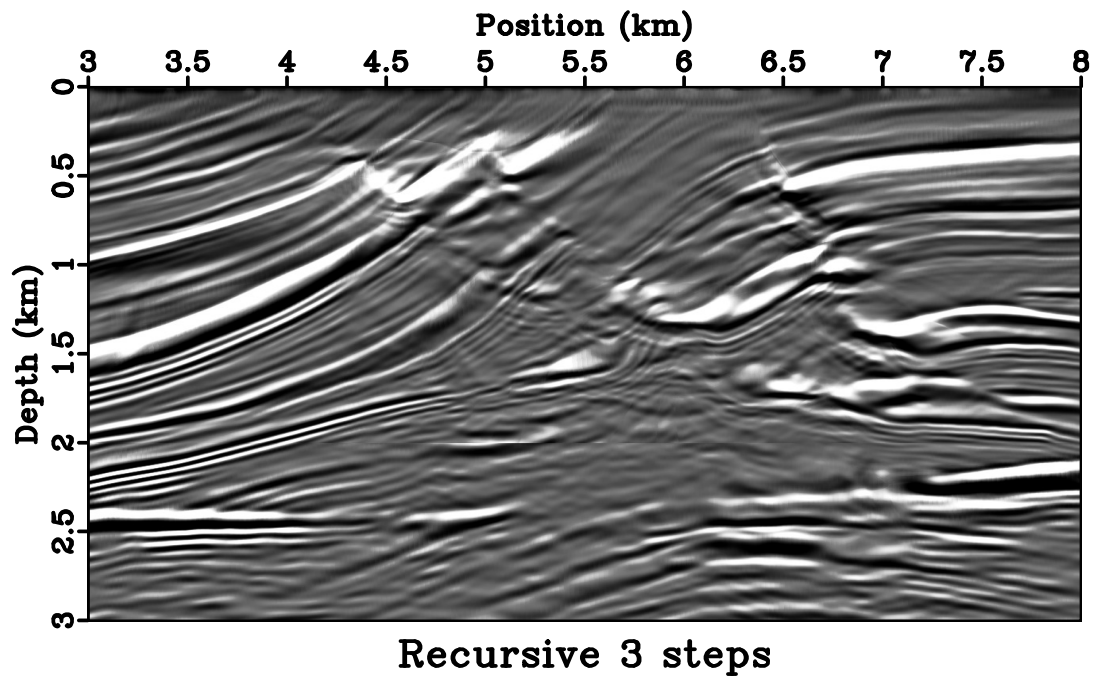


Figure 14: Image of semi-recursive Kirchhoff migration with a three-step redatuming from top surface to 1.5 km depth and a 0.5 km interval each time. The sparse source/receiver sampling is the same as in Figure 13.

DISCUSSION

The proposed approach could be implemented either along with a finite-difference eikonal solver or separately. Our current implementation outputs both traveltime and source-derivative at the same time, with a roughly 30% extra cost per eikonal solve compared to a FMM solver without the source-derivative functionality. An interpolation with these source-derivatives is superior to the ones without and thus enables an accurate traveltime-table compression. For 3D datasets, as both inline and crossline directions may benefit from the source-derivative and interpolation, the overall data compression could be significant. For instance, interpolating 10 shots within each sparse source sampling interval in both inline and crossline directions leads to an approximately 100-fold savings in traveltime storage. The method could be further combined with an interpolation within each source, for example from a coarse grid to a fine grid, for a greater data compression.

While our implementation is for first-arrivals only, the governing equations are valid also for other characteristic branches, for example the most energetic arrivals. However, an underlying assumption of the proposed method is a continuous change in the wave-front of selected arrivals within individual sources. For first-arrivals, this condition always holds valid. However, the most energetic wave-front can be more complicated than that of first-arrival, for example only piece-wise continuous, which may lead to a potential degradation in accuracy. For example, Nichols (1994) showed the most energetic wave-fronts in the Marmousi model. Another assumption is that the traveltime source-derivatives are continuous between nearby sources. This condition breaks down when multi-pathing takes place. Vanelle and Gajewski (2002) suggested to smooth traveltimes around the discontinuities in order to overcome this limitation. In theory, one can try to identify the discontinuities and only perform interpolation within individual continuous pieces by using the eikonal-based source-derivatives. By doing so, one should be able to recover branch jumping in interpolated traveltimes, but only for those locations within the identified continuous pieces. For the discontinuities themselves as well as the gaps between them, additional eikonal solving may be required. An efficient implementation of this strategy remains open for future research.

CONCLUSION

We have shown an application of computing traveltime source-derivatives in Kirchhoff migration. For first-arrivals, a cubic Hermite traveltime interpolation using the first-order source-derivatives speeds up computation and reduces storage without noticeably sacrificing accuracy. Anti-aliasing is another direct application of traveltime source-derivatives that can be easily incorporated into Kirchhoff migration.

Generalization of the method to 3D is straightforward. The computed derivative attributes may benefit other areas besides the kinematic-only Kirchhoff migration shown in this paper. An extension to multi-arrival traveltimes needs further investi-

gation.

ACKNOWLEDGMENTS

We thank the editors, Samuel Gray, and three anonymous reviewers for constructive suggestions that helped improving the quality of the manuscript. We thank Tariq Alkhalifah and Alexander Vladimirsky for useful discussions and sponsors of the Texas Consortium for Computational Seismology (TCCS) for financial support of this research. This publication is authorized by the Director, Bureau of Economic Geology, The University of Texas at Austin.

APPENDIX A

FMM IMPLEMENTATION OF SOURCE-DERIVATIVES

The FMM is a non-iterative eikonal solver with $O(N \log N)$ complexity, where N is the total number of grid points of the discretized domain. It relies on a heap data structure to keep the updating sequence, and a local one-sided upwind finite-difference scheme for ensuring the causality (Sethian, 1996). Consider in 3D a cubic domain discretized into Cartesian grids, with uniform grid size of $(\Delta x, \Delta y, \Delta z)$. Let $\hat{T}_{i,j}^k$ be the traveltime value at vertices $\mathbf{x}_{i,j}^k = (x_i, y_j, z_k)$ and define difference operator D_x^\pm for x direction as

$$D_x^\pm \hat{T}_{i,j}^k = \pm \frac{\hat{T}_{i\pm 1,j}^k - \hat{T}_{i,j}^k}{\Delta x}, \quad (\text{A-1})$$

The causality condition requires picking an upwind neighbor in all directions at $\mathbf{x}_{i,j}^k$.

$$\hat{D}_x \hat{T}_{i,j}^k = \max \left(D_x^- \hat{T}_{i,j}^k, -D_x^+ \hat{T}_{i,j}^k, 0 \right). \quad (\text{A-2})$$

After similar definitions for \hat{D}_y and \hat{D}_z , the local upwind scheme in FMM for equation 3 reads

$$\left(\hat{D}_x \hat{T}_{i,j}^k \right)^2 + \left(\hat{D}_y \hat{T}_{i,j}^k \right)^2 + \left(\hat{D}_z \hat{T}_{i,j}^k \right)^2 = W_{i,j}^k. \quad (\text{A-3})$$

For $\partial \hat{T} / \partial \mathbf{x}$ in equation 6 and $\partial \hat{T} / \partial \mathbf{q}$ in equation 5, we can apply the same upwind strategy:

$$\hat{D}_x \hat{T}_{i,j}^k \cdot \hat{D}_x \left(\frac{\partial \hat{T}}{\partial \mathbf{x}} \right)_{i,j}^k + \hat{D}_y \hat{T}_{i,j}^k \cdot \hat{D}_y \left(\frac{\partial \hat{T}}{\partial \mathbf{x}} \right)_{i,j}^k + \hat{D}_z \hat{T}_{i,j}^k \cdot \hat{D}_z \left(\frac{\partial \hat{T}}{\partial \mathbf{x}} \right)_{i,j}^k = \frac{1}{2} \left(\frac{\partial W}{\partial \mathbf{x}} \right)_{i,j}^k, \quad (\text{A-4})$$

$$\left(\frac{\partial \hat{T}}{\partial \mathbf{q}} \right)_{i,j}^k = \hat{D}_{\mathbf{q}} \hat{T}_{i,j}^k, \quad \mathbf{q} = (x, y, z). \quad (\text{A-5})$$

where in equation A-4 \hat{D}_x , \hat{D}_y and \hat{D}_z are chosen according to $\hat{T}_{i,j}^k$, regardless of $\partial\hat{T}/\partial\mathbf{x}$. Finally,

$$\left(\frac{\partial T}{\partial \mathbf{x}_s}\right)_{i,j}^k = \left(\frac{\partial \hat{T}}{\partial \mathbf{x}}\right)_{i,j}^k - \left(\frac{\partial \hat{T}}{\partial \mathbf{q}}\right)_{i,j}^k. \quad (\text{A-6})$$

To incorporate the computation of traveltime source-derivatives into FMM, one only needs to add equations A-4, A-5 and A-6 after A-3. An extra upwind sorting and solving after pre-computing \hat{T} is not necessary. The total complexity of FMM with the auxiliary output of traveltime source-derivative remains $O(N \log N)$.

APPENDIX B

INTERPOLATION OF SOURCE-DERIVATIVES

Applying the chain-rule 13 to equation 10, we arrive at the interpolation equation for source-derivatives in the cubic Hermite scheme:

$$\begin{aligned} \Delta x_s \frac{\partial T(z,x;z_s,x_s+\alpha\Delta x_s)}{\partial(x_s+\alpha\Delta x_s)} &= (6\alpha^2 - 6\alpha) T(z,x;z_s,x_s) \\ &+ (3\alpha^2 - 4\alpha + 1) \frac{\partial T}{\partial x_s}(z,x;z_s,x_s) \\ &+ (-6\alpha^2 + 6\alpha) T(z,x;z_s,x_s + \Delta x_s) \\ &+ (3\alpha^2 - 2\alpha) \frac{\partial T}{\partial x_s}(z,x;z_s,x_s + \Delta x_s). \end{aligned} \quad (\text{B-1})$$

Analogously, the interpolation of source-derivatives in the linear scheme 11 reads:

$$\Delta x_s \frac{\partial T(z,x;z_s,x_s+\alpha\Delta x_s)}{\partial(x_s+\alpha\Delta x_s)} = -T(z,x;z_s,x_s) + T(z,x;z_s,x_s + \Delta x_s). \quad (\text{B-2})$$

which is a simple first-order finite-difference estimation. Finally, in the case of shift scheme 12, the partial derivative $\partial/\partial\alpha$ must be applied to the shifted traveltime terms at the same time:

$$\begin{aligned} \Delta x_s \frac{\partial T(z,x;z_s,x_s+\alpha\Delta x_s)}{\partial(x_s+\alpha\Delta x_s)} &= -T(z,x - \alpha\Delta x_s;z_s,x_s) \\ &- (1 - \alpha)\Delta x_s \frac{\partial T(z,x-\alpha\Delta x_s;z_s,x_s)}{\partial(x-\alpha\Delta x_s)} \\ &+ T(z,x + (1 - \alpha)\Delta x_s;z_s,x_s + \Delta x_s) \\ &- \alpha\Delta x_s \frac{\partial T(z,x+(1-\alpha)\Delta x_s;z_s,x_s+\Delta x_s)}{\partial(x+(1-\alpha)\Delta x_s)}. \end{aligned} \quad (\text{B-3})$$

The required spatial derivatives can be estimated from the traveltime table by means of finite-differences, for example by using the upwind approximation A-2.

REFERENCES

- Abma, R., J. Sun, and N. Bernitsas, 1999, Antialiasing methods in Kirchhoff migration: *Geophysics*, **64**, 1783–1792.
- Albertin, U., D. Yingst, P. Kitchenside, and V. Tcheverda, 2004, True-amplitude beam migration: 68th Annual International Meetings, SEG Expanded Abstracts, 949–952.

- Aldridge, D. F., 1994, Linearization of the eikonal equation (short note): *Geophysics*, **59**, 1631–1632.
- Alkhalifah, T., 2011, Efficient traveltime compression for 3-D prestack Kirchhoff migration: *Geophysical Prospecting*, **59**, 1–9.
- Alkhalifah, T., and S. Fomel, 2010, An eikonal based formulation for traveltime perturbation with respect to the source location: *Geophysics*, **75**, no. 6, T175–T183.
- Bevc, D., 1997, Imaging complex structures with semirecursive Kirchhoff migration: *Geophysics*, **62**, 577–588.
- Bortfeld, R., 1989, Geometrical ray theory: rays and traveltimes in seismic systems (second-order approximation of traveltimes): *Geophysics*, **54**, 342–349.
- Chapman, C., 2004, *Fundamentals of seismic wave propagation*: Cambridge University Press.
- Dellinger, J. A., S. H. Gray, G. E. Murphy, and J. T. Etgen, 2000, Efficient 2.5-D true-amplitude migration: *Geophysics*, **65**, 943–950.
- Engquist, B., and O. Runborg, 1996, Multi-phase computations in geometrical optics: *Journal of Computational and Applied Mathematics*, **74**, 175–192.
- Fomel, S., 2002, Antialiasing of Kirchhoff operators by reciprocal parameterization: *Journal of Seismic Exploration*, **10**, 293–310.
- Fomel, S., S. Luo, and H. Zhao, 2009, Fast sweeping method for the factored eikonal equation: *Journal of Computational Physics*, **228**, 6440–6455.
- Fomel, S., and J. A. Sethian, 2002, Fast phase-space computation of multiple arrivals: *Proceedings of the National Academy of Sciences*, **99**, 7329–7334.
- Franklin, J. B., and J. M. Harris, 2001, A high-order fast marching scheme for the linearized eikonal equation: *Journal of Computational Acoustics*, **9**, 1095–1109.
- Geoltrain, S., and J. Brac, 1993, Can we image complex structures with first-arrival traveltime?: *Geophysics*, **58**, 564–575.
- Gray, S. H., 2005, Gaussian beam migration of common-shot records: *Geophysics*, **70**, S71–S77.
- Hill, N. R., 1990, Gaussian beam migration: *Geophysics*, **55**, 1416–1428.
- , 2001, Prestack Gaussian beam depth migration: *Geophysics*, **66**, 1240–1250.
- Lumley, D. E., J. F. Claerbout, and D. Bevc, 1994, Anti-aliased Kirchhoff 3-D migration: 64th Annual International Meetings, SEG Expanded Abstracts, 1282–1285.
- Mendes, M., 2000, Green’s function interpolation for prestack imaging: *Geophysical Prospecting*, **48**, 49–62.
- Nichols, D. E., 1994, *Imaging complex structures using band-limited Green’s functions*: PhD thesis, Stanford University.
- Press, W. H., S. A. Teukolsky, W. T. Vetterling, and B. P. Flannery, 2007, *Numerical recipes: The art of scientific computing*: Cambridge University Press.
- Qian, J., and W. W. Symes, 2002, An adaptive finite-difference method for traveltimes and amplitudes: *Geophysics*, **67**, 167–176.
- Sava, P., and S. Fomel, 1998, Huygens wavefront tracing: A robust alternative to ray tracing: 62nd Annual International Meetings, SEG Expanded Abstracts, 1961–1964.
- Sethian, J. A., 1996, *Level set methods: Evolving interfaces in geometry, fluid mechanics, computer vision, and materials science*: Cambridge University Press.

- Sethian, J. A., and A. M. Popovici, 1999, 3-D imaging using higher order fast marching traveltimes: *Geophysics*, **64**, 516–523.
- Slotnick, M. M., 1959, *Lessons in seismic computing*: Society of Exploration Geophysics.
- Symes, W. W., and J. Qian, 2003, A slowness matching Eulerian method for multivalued solutions of eikonal equations: *Journal of Scientific Computing*, **19**, 501–526.
- Ursin, B., 1982, Quadratic wavefront and traveltime approximations in inhomogeneous layered media with curved interfaces: *Geophysics*, **47**, 1012–1021.
- Vanelle, C., and D. Gajewski, 2002, Second-order interpolation of traveltimes: *Geophysical Prospecting*, **50**, 73–83.
- Vanelle, C., M. Spinner, T. Hertweck, C. Jäger, and D. Gajewski, 2006, Traveltime-based true-amplitude migration: *Geophysics*, **71**, no. 6, S251–S259.
- Červený, V., 2001, *Seismic ray theory*: Cambridge University Press.
- Versteeg, R., 1994, The Marmousi experience: Velocity model determination on a synthetic complex data set: *The Leading Edge*, **13**, 927–936.
- Xu, S., H. Chauris, G. Lambaré, and M. Noble, 2001, Common-angle migration: A strategy for imaging complex media: *Geophysics*, **66**, 1877–1894.
- Zhao, H. K., 2005, A fast sweeping method for eikonal equations: *Mathematics of Computation*, **74**, 603–627.